RSC Advances




ROYAL SOCIETY OF CHEMISTRY

www.rsc.org/advances

# Electrochemical mechanism of Cr(III) reduction for preparing crystalline chromium coatings based on 1-butyl-3-methylimidazolium hydrogen sulfate ionic liquid

Xinkuai He, Chen Li, Qingyun Zhu, Bailong Hou, Yumei Jiang, Luye Wu *

School of Packaging and Materials Engineering, Hunan University of Technology, Zhuzhou 412007, P. R. China.

*Corresponding author

E-mail: lyxk999@163.com (L.Y. Wu) and h-xk@163.com (X.K. He)

Phone: +86 731 22182088, Fax: +86 731 22182168

Chromium coatings can be prepared from ionic liquids containing Cr(III) ions. However, these coatings are almost amorphous due to the fact that the deposits include metalloid atoms (such as P, C, N, O). The present work reports the direct preparation of crystalline chromium coatings by electrodeposition based on 1-butyl-3-methylimidazolium hydrogen sulfate ([BMIM]$HSO_4$) ionic liquid. The Cr(III) electrochemical reduction mechanism and chromium nucleation/growth process on a glassy carbon (GC) electrode in [BMIM]$HSO_4$ are investigated. These results from cyclic voltammetry and linear sweep voltammetry reveal that the Cr(III) reduction occurs by a two-step process, Cr(III) to Cr(II), and Cr(II) to Cr(0), respectively, the first step is irreversible with a diffusion coefficient of Cr(III) in solution of $2.03 \times 10^{-7}$ $cm^2 \cdot s^{-1}$ at 353 K, and the two-step process has been confirmed by chronopotentiometry. The chromium coatings are characterized by SEM, EDS and XRD. XRD pattern of the coatings shows the characteristic peak of crystal Cr. Chronoamperometry results reveal that chromium electrodeposition in [BMIM]$HSO_4$ can be attributed to a three-dimensional instantaneous nucleation and diffusion-controlled growth mechanism. These results observed in this work indicate that [BMIM]$HSO_4$ ionic liquid may be a useful electrolyte for chromium electrodeposition.

## 1. Introduction

The electrodeposition of chromium and its alloys is of great practical importance due to the fact that these coatings are widely used in industrial fields such as corrosion prevention, electronic materials, and functional coatings.[1-5] Chromium plating is

traditionally prepared in aqueous solutions.[6-12] However, the chromium electrodeposition from Cr(III)-based aqueous baths is generally accompanied by intensive hydrogen evolution reaction. Thus, the current efficiency and quality of the chromium deposits can be obviously affected by the reaction.[6, 13, 14] Another important issue concerning the technique is the participation in the chromium deposition process of organic additives, which is normally used in Cr(III)-based aqueous baths.[15-18] The participation results in the formation of chromium carbide compounds in these deposits, suggesting that they are normally amorphous.[15-17] However, the crystal chromium coatings present higher hardness, better wear resistance, and then more extensive applications. For these reasons it is of great interest to find alternative electrolytes for crystalline chromium electrodeposition. Compared to aqueous solutions, ionic liquids are an ideal kind of solvents for the electrodeposition of metals and alloys due to the fact that they can provide a wide electrochemical window, good electrical conductivity and low volatility for electrolysis without evolution of hydrogen.[19-26]

In the last two decades, the electrodeposition of chromium and its alloys from ionic liquids is popular. For instance, Al-Cr alloy coatings were prepared by Moffat[27] and Ali et al.[28] in $AlCl_3$-trimethylphenylammonium chloride (TMPAC) or in $AlCl_3$-N-(n-butyl)pyridinium chloride containing Cr(II) ions. Moreover, chromium concentrations of these Al-Cr alloys, between 0 and 94 at.%, could be adjusted by the applied process parameters. Whereas, the reductive Cr(II) as a chromium source was used for these Al-Cr alloys electrodeposition in the above two ionic liquids.[27, 28] In

contrast to Cr(II), the electrodeposition of chromium and its alloys using Cr(III) is more popular due to its better chemical stability. For instance, the crack-free chromium coatings were electrodeposited by Abbott and his co-workers from choline chloride/chromium chloride system.[29] But its hardness is only 242 Vickers, which is less than that of the chrome hydride electrodeposited from chromic acid process (typically 800 to 900 Vickers). Similarly, microcrack chromium coatings could be prepared based on choline chloride/chromium chloride system.[30] To improve these chromium coatings quality, a new ionic liquid, 1-butyl-3-methylimidazolium tetrafluoroborate ([BMIM]$BF_4$), was applied to prepare black chromium coatings by Eugénio et al.[31, 32]. It should be noted that these chromium coatings were composed of a mixture of chromium oxide/hydroxide and metallic chromium with a sub-micrometric granular structure. Thus, these coatings are amorphous. In addition, they found that the Cr(III) reduction is quasi-reversible and occurs in a two-step process, Cr(III) to Cr(II) and Cr(II) to Cr(0).[32] However, the Cr(III) reduction in [BMIM]$PF_6$ is an irreversible one-step reaction, Cr(III) to Cr(0).[33] It can be concluded that the mechanism of Cr(III) reduction may be remarkably different in different ionic liquids. It should be noted that these chromium coatings electrodeposited from the two ionic liquids are amorphous due to the fact that they include P, C and O atoms. It suggests that [BMIM]$BF_4$ and [BMIM]$PF_6$ are not stable enough and can involve in the electrodepositing process. Thus, it is important to develop a more stable ionic liquid system from which the crystalline chromium coatings can be prepared directly.

Moreover, the electrocrystallization mechanism of chromium depositing from ionic liquid systems has scarcely been investigated. The metallic phase growth is preceded by the nucleation step. The nucleation theory of metals on surfaces proposed by Scharifker and Hills[34-36] was acknowledged for the examination of the process of metals electrodeposition from aqueous solutions[37-39] and ionic liquids[40-42]. For instance, the nucleation and growth mechanism of sliver from $10^{-2}$ M $Ag(NH_3)^{2+}$/1.6 M $NH_3$, 1 M $KNO_3$ onto different carbon electrode substrates has been successfully determined by Miranda et al.[43] and its behavior is in accordance with a three-dimensional (3D) instantaneous nucleation mechanism followed by growth of the nuclei controlled by silver ions diffusion kinetic.

1-butyl-3-methylimidazolium-hydrogen sulfate ([BMIM]$HSO_4$) ionic liquid may not involve in the chromium electrodeposition process since it can provide a more stable anion that is not subject to decomposition as has been observed with the fluorinated anions such as $[BF_4]^-$ and $[PF_6]^-$.[44, 45] In addition, the crystalline chromium prepared directly from 1-butyl-3-methylimidazolium hydrogen sulfate still has not been reported. Thus, in this work, [BMIM]$HSO_4$ is used as the electrolyte to prepare the crystalline chromium coatings. The electrochemical reduction of Cr(III) on a GC electrode is investigated by cyclic voltammetry, linear sweep voltammetry. Moreover, the result is confirmed by chronopotentiometry, and the morphology and structural properties of the obtained coatings are also characterized by SEM, EDS and XRD. Finally, the chromium nucleation/growth process is investigated by chronoamperometry.

# 2. Experimental

## 2.1 Materials

The $[BMIM]HSO_4$ was synthesized and purified according to the method published in a previous literature.[46] The 0.55 M $CrCl_3$-$[BMIM]HSO_4$ solutions were prepared by heating the proper mixtures of anhydrous $CrCl_3$(99.9%, Aldrich) and $[BMIM]HSO_4$ in a beaker for 72 h, the process was performed in a glove box. The working electrode was GC purchased from Alfa Aesar with a purity of 99.99% and the exposing area was 0.07 $cm^2$.

## 2.2 Measurement procedures and apparatus

Electrochemical measurements were performed by a CHI 660B potentiostat using three-electrode configuration. The GC mentioned above was used as the working electrode. A platinum foil (20 mm × 15 mm) and a platinum electrode were used as the counter-electrode and the reference electrode, respectively. The electrolyte temperature was maintained at 353 K during the electrochemical measurements. The working electrode was mechanically polished with 0.05 μm alumina slurries on lapping pads. All the electrodes were rinsed by deionised water then carefully dried with $N_2$ before transported into the glove box. It should be noted that the Tafel curves were obtained at a scan rate of 1.0 $mV \cdot s^{-1}$ around -150 mV against the equilibrium potential.

## 2.3 Electrodeposition

For electrodeposition, a platinum foil (20 mm × 15 mm) was used as anode and a Cu foil (10 mm × 5 mm, 99.9%) as cathode, respectively. A platinum electrode was

connected as the reference electrode, to which all potentials were referred. The distance between the cathode and anode was maintained at 30 mm. After electrodeposition, the samples were cleaned in acetone to eliminate the [BMIM]$HSO_4$ remains, and then rinsed in deionized water. Thickness of Cr films was calculated according to the gravimetric data $\Delta M$ using the equation: $T = \frac{\Delta M}{\rho \cdot S}$, where $T$ is the coating thickness, $\Delta M$ is the weight gained on the Cu substrate which can be measured, $\rho$ is the density of chromium(7.20 g·cm$^{-3}$), $S$ is the surface area of Cu substrate that involved in the electrodeposition process.

### 2.4 Characterization of the electrodeposited coatings

The surface morphology of the chromium coatings was observed by a SEM (HITACHI S-3000N), provided with an energy dispersive spectrometer (EDS) detector. X-ray diffractogram (XRD) was recorded using a Siemens D-5000 diffractometer with $CuK_\alpha$ radiation.

## 3. Results and discussion

### 3.1 Cyclic voltammetry study

Transient cyclic voltammogram is an effective technique applied to obtain important information about the reaction on a GC electrode surface.[32, 47] To study the electrochemical reduction of Cr(III), electrochemical measurements are performed at 353 K using this technique. A representative cyclic voltammogram of pure [BMIM]$HSO_4$ is shown in Fig. 1 (curve a). No apparent reduction peak is observed in the forward scan up to -3.10 V and no anodic peak is observed in the reverse scan. The result indicates that [BMIM]$HSO_4$ is electrochemically stable in the potential

144 ranging from -3.10 to -0.10 V, which means [BMIM]$HSO_4$ possesses an
145 electrochemical window of 3.0 V, in accordance with a previous literature.[48]
146 The typical cyclic voltammogram of 0.55 M Cr(III) in [BMIM]$HSO_4$ ionic liquid
147 on the GC electrode at 353 K is also presented in Fig. 1 (curve b). The potential scan
148 is negatively begun from 0.25 to -2.45 V, and then reversed to the beginning potential.
149 Two obvious peaks are observed at -1.60 and -2.25 V, implying that the Cr(III)
150 reduction occurs in two steps via Cr(II) ions:
151 peak A $Cr(\mathrm{III}) + 1e^- \rightarrow Cr(\mathrm{II})$
152 peak B $Cr(\mathrm{II}) + 2e^- \rightarrow Cr(0)$
153 It is a widely recognized mechanism for the Cr(III) reduction, in accordance with the
154 published literatures.[32, 49]
155 The effect of the potential scan rates on the voltammograms of the electrolyte
156 corresponding to different scan ranges is displaced in Fig. 2. As shown in Fig. 2, the
157 voltammograms of the electrode is changed remarkably by scan rate. The cathodic
158 peak potential shifts negatively and the peak current increases with the increasing of
159 the scan rate. In addition, whether or not substep scan, no obvious anodic peaks are
160 observed in the reverse scan. These results also indicate that the reduction of Cr(III) in
161 [BMIM]$HSO_4$ on a GC electrode is an irreversible two-step reaction, which is also
162 verified by the linear relationship between the peak potential $E_p$ ($E_{pA}$ and $E_{pB}$) and ln$v$
163 (Fig. 3a and b). However, the reduction of Cr(III) to Cr(II) in [BMIM][$BF_4$] on a GC
164 electrode is a quasi-reversible reaction,[34] the difference may be attributed to the
165 diversity of properties between the $[HSO_4]^-$ and $[BF_4]^-$ in ionic liquid solutions.

For an irreversible process, there is a relationship between $n_\alpha$ and $|E_p-E_{p/2}|$:[50]

$$| E_p-E_{p/2}| = 1.857RT/(\alpha n_\alpha F) \quad (1)$$

where $E_p$ is the peak potential, $E_{p/2}$ is the half-peak potential, $T$ is the absolute temperature, $R$ is the gas constant, $F$ is the Faraday constant, $n_\alpha$ is the number of electrons in the rate determining step and $\alpha$ is the charge transfer coefficient. Thus, the value of $n_\alpha$ for the irreversible process can be determined by Eq.(1). The average value of $\alpha n_\alpha$ is found to be 0.250 at 353 K. Thus, considered that $\alpha n_\alpha \leq 1$, it is inferred that the number of electrons participated in the kinetic step is one, with $\alpha = 0.250$, which is in accordance with the previous literature.[49]

Fig. 4 presents the linear relationship between the cathodic peak current ($I_{pA}$) and $v^{1/2}$, implying the Cr(III) reduction is controlled by a diffusion process in [BMIM]$HSO_4$ ionic liquid. Thus, based on the above discussion, it can be surmised that the reduction of Cr(III) to Cr(II) is an irreversible and diffusion-controlled process. By supposing the reaction is completely irreversible and ignoring the electrode area change caused by chromium electrodeposition, the diffusion coefficient of Cr(III) in [BMIM]$HSO_4$ solution at 353 K can be calculated using Eq.(2):[51]

$$I_p = 0.4958nF^{3/2}C_0AD^{1/2}v^{1/2}(\alpha n_\alpha/RT)^{1/2} \quad (2)$$

where $A$ is the geometric area of the electrode, $C_0$ is the Cr(III) concentration, $D$ is the diffusion coefficient, $\alpha$ is the charge transfer coefficient, $n_\alpha$ is the number of electrons in the rate determining step, $v$ is the potential scan rate and $n$ is the number of electrons transferred. The average value of $\alpha n_\alpha$ can be estimated using Eq.(1) and according to Eq.(2), the diffusion coefficient of Cr(III) in $CrCl_3$-[BMIM]$HSO_4$

188 solution is calculated. Thus, the diffusion coefficient of Cr(III) obtained at 353 K is
189 $2.03 \times 10^{-7}$ $cm^2$ $s^{-1}$.

190 **3.2 Linear sweep voltammetry study**

191 A linear sweep voltammetry measurement using a lower sweep rate is carried out
192 in order to further confirm the electrochemical mechanism of Cr(III) reduction. Fig.
193 5a presents a typical linear sweep voltammogram of GC electrode in 0.55 M Cr(III)-
194 [BMIM]$HSO_4$ solution with a scan rate of 1 $mV \cdot s^{-1}$ at 353 K. As shown in Fig. 5a,
195 almost no increase of cathodic current occurs before -0.89 V (region 'A'). The current
196 begins rising remarkably from -0.89 to -1.67 V (region 'B'), suggesting that the
197 Cr(III) reduction has happened. In order to obtain more information about the
198 reduction reaction, another electrodepositing experiment on a copper substrate based
199 on 0.55 M Cr(III)-[BMIM]$HSO_4$ solution at a constant potential of -1.67 V for 30 min
200 is carried out at 353 K. No deposits are observed at the potential. The result can be
201 attributed to the reduction of Cr(III) to Cr(II), implying that the reduction of Cr(II) to
202 Cr(0) does not happen. The cathodic current begins rising more sharply from -1.67 to
203 -2.15 V (region 'C'), which indicates that another reduction reaction occurs. To
204 further confirm the reduction reaction, another electrodepositing experiment under the
205 same conditions is carried out at -2.00 V. Deposits are observed at the potential,
206 implying that the reduction reaction of Cr(II) to Cr(0) also happens. Thus, these
207 results are consistent with cyclic voltammetry. In addition, these deposits are
208 investigated by SEM, EDS and XRD. As shown in Fig. 6a, a ball-like structure
209 without obvious micro cracks and pinholes is observed. The structure is clearly

defined at a higher resolution (Fig. 6b). EDS analysis shows that the deposits are composed of Cr without other elements (Fig. 6c), and the XRD pattern shows two strong peaks for (210) and (200) planes locate at 2θ = 44.02° and 64.58°, respectively, which reveals that the Cr electrodeposits present a crystal structure with preferential orientation (210) and (200) (Fig. 6d). It should be noted that the thickness of the deposits can be up to 9.2 μm, which is calculated by the equation: $T = \frac{\Delta M}{\rho \cdot S}$.

However, these chromium deposits obtained from [BMIM]$BF_4$ or [BMIM]$PF_6$ ionic liquid containing Cr(III) ions are generally amorphous.[32, 33] To prepare the crystalline coatings, further annealing to the amorphous deposits at high temperature is integrant.[15-17] Thus, the technique using [BMIM]$HSO_4$ as Cr(III) electrolytes to prepare crystalline chromium coatings directly is simpler, which also demonstrates that [BMIM]$HSO_4$ ionic liquid in commercial chromium plating is more promising. In addition, as shown in Fig. 5b, a Tafel line is observed in the potential ranging from -0.98 to -1.03 V when log$I$ is plotted against $E$, corresponding well to the result of the Cr(III) reduction. Thus, the cathode transfer coefficient can be determined by Eq. (3).[52]

$$b_c = 2.3RT/\alpha nF \quad (3)$$

where $b_c$ is the slope of Tafel line, $R$ is the ideal gas constant, $F$ is the Faraday constant, $T$ is the absolute temperature, $\alpha$ is the cathode transfer coefficient, $n$ is the number of electrons transferred. The cathode transfer coefficient is 0.241, which is basically in accordance with that obtained from cyclic voltammetry.

### 3.3 Chronopotentiometry study

The characteristics of chronopotentiometry about a two-step reaction have been reported by Plonski[53] and its most acknowledged characteristics can be described using the theoretical curves given in Fig. 7a. Three main observations are made: (i) as a result of the competition between the charging of the double layer and the transitory electron transfer process, the $\eta$-$t$ curves are peak-shaped between $i_{cr1}$ and $i_{cr2}$ ($\eta$ is the overvoltage, $i$ is the current); (ii) at first, the difference $\eta_{peak}$-$\eta_x$ increases and passes through a maximum value, when $i \rightarrow i_{cr2}$, the value decreases toward zero; (iii) it is generally valid that the time necessary to reach the steady state decreases with the increasing of $i$, except for $i_{cr2}$ when the steady state of $\eta$ attains sooner. However, for a one-step reaction, $\eta$ is only monotonous change with the time.[53]

In order to further investigate whether the Cr(III) reduction is a two-step process, chronopotentiometric measurements are carried out in 0.55 M Cr(III)-[BMIM]$HSO_4$ solutions by stepping the current density from $5.0 \times 10^{-3}$ to $5.6 \times 10^{-3}$ A, which are within the theoretical value ranging between $2.09 \times 10^{-4}$ and $5.80 \times 10^{-3}$ A (Fig. 7a). Representative potential-time transients resulting from these measurements are depicted in Fig. 7b. These transient plots present the above similar characteristics of the theoretical curves, which implies that Cr(III) reduction is a two-step process.

### 3.4 Chronoamperometry study

Chronoamperometric experiments are performed to reveal the mechanism of chromium nucleation/growth process in 0.55 M Cr(III)-[BMIM]$HSO_4$ system by stepping the potentials from -1.90 to -2.00 V. Fig. 8a shows three representative current-time transients resulting from these experiments that exhibit a typical shape

for a diffusion-limited nucleation process with three-dimensional (3D) growth of nuclei. Upon the potential step, the current-transients are characterized by a shape double-layer charging current decay followed by a rising current due to the formation and growth of Cr nuclei until a current maximum, $I_{max}$, is reached at a time, $t_{max}$ (i.e. the Cr nuclei begin to overlap, then follow by a decaying portion, converging to a limiting current corresponding to linear diffusion of the electroactive ions to a planar electrode as per the Cottrell equation). The $I_{max}$ increases while the $t_{max}$ shortens when increasing the applied nucleation potential (Fig. 8a). This can be attributed to the decreasing in the time required for the diffusion layer to overlay due to an increased nucleation density.[54] The electrodeposition of metals onto foreign surfaces often presents some type of 3D nucleation. Two limiting cases for this type of metal deposition have been classified by Scharifker and Hills as progressive nucleation, where the number of nuclei increases during the whole depositing process, and instantaneous nucleation, where all nuclei are formed immediately after the potential step.[34-36] To confirm the nucleation behaviors, the $I$ versus $t$ transients are converted to dimensionless $(I/I_{max})^2$ versus $(t/t_{max})$ curves and compared with the theoretical dimensionless curves developed by Scharifker et al.[53] for the 3D instantaneous (Eq.(4)) and progressive (Eq.(5)) nucleation.[34]

$$\frac{I^2}{I_{max}^2} = \frac{1.9542}{t/t_{max}}\left[1-\exp\left(-1.2564\frac{t}{t_{max}}\right)\right]^2 \qquad (4)$$

(Instantaneous nucleation)

$$\frac{I^2}{I_{max}^2} = \frac{1.2254}{t/t_{max}}\left[1-\exp\left(-2.3367\frac{t^2}{t_{max}^2}\right)\right]^2 \quad (5)$$

(Progressive nucleation)

where $I$ and $t$ are the current and time, respectively, and $I_{max}$ is the maximum current at time $t_{max}$. As the experimental and theoretical plots represented in Fig. 8b, the chromium electrodeposition on a GC electrode in [BMIM]$HSO_4$ ionic liquid most likely involves in the 3D instantaneous nucleation mode.

As depicted in Fig. 8c, the current-time transients in Fig. 8a suggest that the growth of chromium nuclei on a GC electrode is typical for a diffusion-controlled process since after $I_{max}$, all of the decreasing currents $I$ present a good linear relation with $t^{-1/2}$. It can be concluded from the above results that the Cr(III) reduction on a GC electrode corresponds to a 3D instantaneous nucleation with diffusion-controlled growth. In addition, the diffusion coefficient ($D$) can be calculated using the Cottrell equation:[55]

$$I = nFAD^{1/2}C_0/(\pi^{1/2}t^{1/2}) \quad (6)$$

where $F$ is the Faraday constant, $n$ is the number of electrons transferred, $A$ is the geometric area of the electrode, $C_0$ is the Cr(III) concentration, $D$ is the diffusion coefficient. Thus, the diffusion coefficient determined by the slope of the plot of $I$ versus $t^{-1/2}$ (line 1 in Fig. 8c) is about $1.98 \times 10^{-7}$ $cm^2 \cdot s^{-1}$, which is basically consistent with that obtained from cyclic voltammetry.

## 4. Conclusions

The Cr(III) electrochemical reduction on a GC electrode in $[BMIM]HSO_4$ ionic liquid is studied. The cyclic voltammograms of Cr(III) at different scan rates are measured. The result reveals that the Cr(III) reduction occurs in a two-step, which is an irreversible and diffusion-controlled process. The diffusion coefficient of Cr(III) in $[BMIM]HSO_4$ solution obtained from cyclic voltammetry is $2.03 \times 10^{-7}$ $cm^2 \cdot s^{-1}$ at 353 K. The two-step reaction is also confirmed by chronopotentiometry. Moreover, it can be concluded that the chromium electrodeposition proceeds through a 3D nucleation growth mechanism as deduced by analysis of chronoamperometry data. XRD pattern of the electrodeposited chromium layer presents the characteristic peak of crystal Cr. These results obtained in this work indicate that the $[BMIM]HSO_4$ ionic liquid may be a useful electrolyte for electrodeposition of metals.

## Acknowledgments

The authors acknowledge the financial supports of the Natural Science Foundation of China (No. 21476067), the Natural Science Foundation of Hunan Province, China (Nos.2015JJ2044 and 13JJ3107), and the Project Sponsored by the Scientific Research Foundation for the Returned Overseas Chinese Scholars, State Education Ministry.

## References

1 C. E. Lu, N. W. Pu, K. H. Hou, C. C. Tseng and M. D. Ger, *Appl. Surf. Sci.*, 2013, **282**, 544-551.

2 Z. X. Zeng, Y. L. Sun and J. Y. Zhang, *Electrochem. Commun.*, 2009, **11**, 331-334.

316 3 K. N. Sun, X. N. Hu, J. H. Zhang and J. R. Wang, *Wear*, 1996, **196**, 295-297.

317 4 X. K. He, B. L. Hou, Y. X. Cai, C. Li, Y. M. Jiang and L. Y. Wu, *J. Nanosci.*

318 *Nanotechno.*, 2013, **13**, 4031-4039.

319 5 X. K. He, B. L. Hou, Y. X. Cai and L. Y. Wu, *J. Nanosci. Nanotechno.*, 2013, **13**,

320 2193-2200.

321 6 Y. B. Song and D. T. Chin, *Electrochim. Acta*, 2002, **48**, 349-356.

322 7 V. Protsenko and F. Danilov, *Electrochim. Acta*, 2009, **54**, 5666-5672.

323 8 Z. X. Zeng, Y. X. Zhang, W. J. Zhao and J. Y. Zhang, *Surf. Coat. Tech.*, 2011,

324 **205**, 4771-4775.

325 9 V. S. Protsenko, F. I. Danilov, V. O. Gordiienko, S. C. Kwon, M. Kim and J. Y.

326 Lee, *Thin Solid Films*, 2011, **520**, 380-383.

327 10 R. Giovanardi and G. Orlando, *Surf. Coat. Tech.*, 2011, **205**, 3947-3955.

328 11 Z. A. Hamid, *Surf. Coat. Tech.*, 2009, **203**, 3442-3449.

329 12 N. V. Phuong, S. C. Kwon, J. Y. Lee, J. Y. Shin, B. T. Huy and Y. I. Lee,

330 *Microchem. J.*, 2011, **99**, 7-14.

331 13 N. V. Phuong, S. C. Kwon, J. Y. Lee, J. H. Lee and K. H. Lee, *Surf. Coat. Tech.*,

332 2012, **206**, 4349-4355.

333 14 V. S. Protsenko, V. O. Gordiienko, F. I. Danilov and S. C. Kwon, *Metal Finishing*,

334 2011, **109**, 33-37.

335 15 O. V. Safonova, L. N. Vykhodtseva, N. A. Polyakov, J. C. Swarbrick, M. Sikora,

336 P. Glatzel and V. A. Safonov, *Electrochim. Acta*, 2010, **56**, 145-153.

337 16 V. A. Safonov, L. N. Vykhodtseva, Y. M. Polukarov, O. V. Safonova, G.

338 Smolentsev, M. Sikora, S. G. Eeckhout and P. Glatzel, *J. Phys. Chem. B*, 2006,

339 **110**, 23192-23196.

17 S. G. Eeckhout, O. V. Safonova, G. Smolentsev, M. Biasioli, V. A. Safonov, L. N. Vykhodtseva, M. Sikora and P. Glatzel, *J. Anal. Atom. Spectrom.*, 2009, **24**, 215-223.

18 F. I. Danilov and V. S. Protsenko, *Prot. Met.*, 2001, **37**, 223-228.

19 A. P. Abbott and K. J. McKenzie, *Phys. Chem. Chem. Phys.*, 2006, **8**, 4265-4279.

20 K. R. Seddon, G. Srinivasan, M. Swadźba-Kwaśny and A. R. Wilson, *Phys. Chem. Chem. Phys.*, 2013, **15**, 4518-4526.

21 Y. H. You, C. D. Gu, X. L. Wang and J. P. Tu, *J. Electrochem. Soc.*, 2012, **159**, 642-648.

22 C. D. Gu and J. P. Tu, *Langmuir*, 2011, **27**, 10132-10140.

23 C. D. Gu, Y. H. You, Y. L. Yu, S. X. Qu and J. P. Tu, *Surf. Coat. Tech.*, 2011, **205**, 4928-4933.

24 M. C. Buzzeo, R. G. Evans and R. G. Compton, *Chem. Phys. Chem.*, 2004, **5**, 1106-1120.

25 Q. B. Zhang and Y. X. Hua, *Mater. Chem. Phys.*, 2012, **134**, 333-339.

26 Q. B. Zhang, Y. X. Hua, Y. T. Wang, H. J. Lu and X. Y. Zhang, *Hydrometallurgy*, 2009, **98**, 291-297.

27 T. P. Moffat, *J. Electrochem. Soc.*, 1994, **141**, 115-117.

28 M. R. Ali, A. Nishikata and T. Tsuru, *Electrochim. Acta*, 1997, **42**, 2347-2354.

29 A. P. Abbott, G. Capper, D. L. Davies and R. K. Rasheed, *Chem-Eur. J.*, 2004, **10**, 3769-3774.

30 Y. Cui and Y. X. Hua, *T. Nonferr. Metal.*, 2011, **63**, 92-96.

31 S. Eugénio, C. M. Rangel, R. Vilar and A. M. B. Rego, *Thin Solid Films*, 2011, **519**, 1845-1850.

32 S. Eugénio, C. M. Rangel, R. Vilar and S. Quaresma, *Electrochim. Acta*, 2011, **56**, 10347-10352.

33 Y. S. J. Hasimu, R. Q. Liu and H. Y. Mi, *Chem. J. Chinese U.*, 2014, **35**, 140-145.

34 B. Scharifker and G. Hills, *Electrochim. Acta*, 1983, **28**, 879-889.

35 G. Gunawardena, G. Hills and I. Montenegro, *J. Electroanal. Chem.*, 1982, **138**, 241-254.

36 B. R. Scharifker and J. Mostany, *J. Electroanal. Chem.*, 1984, **177**, 13-23.

37 M. M. Hernandez, I. Gonzalez and N. Batina, *J. Phys Chem B*, 2001, **105**, 4214-4223.

38 K. Yao and Y. F. Cheng, *Int. J. Hydrogen Energ.*, 2008, **33**, 6681-6686.

39 T. Rapecki, Z. Stojek and M. Donten, *Electrochim. Acta*, 2013, **106**, 264-271.

40 R. Bomparola, S. Caporali, A. Lavacchi and U. Bardi, *Surf. Coat. Tech.*, 2007, **201**, 9485-9490.

41 M. Jayakumar, K. A. Venkatesan, T. G. Srinivasan and P. R. Vasudeva Rao, *Electrochim. Acta*, 2009, **54**, 6747-6755.

42 A. Bakkar and V. Neubert, *Electrochim. Acta*, 2013, **103**, 211-218.

43 R. Bomparola, S. Caporali, A. Lavacchi and U. Bardi, *Surf. Coat. Tech.*, 2007, **201**, 9485-9490.

44 R. P. Swatloski, J. D. Holbrey and R. D. Rogers, *Green Chem.*, 2003, **5**, 361-363.

45 A. J. Whitehead, A. G. Lawrance and A. McCluskey, *Green Chem.*, 2004, **6**, 313-315.

46 J. A. Whitehead, G. A. Lawrance and A. McCluskey, *Aust. J. Chem.*, 2004, **57**, 151-155.

47 E. S. C. Ferreira, C. M. Pereira and A. F. Silva, *J. Electroanal. Chem.*, 2013, **707**, 52-58.

389 48 F. Endres, S. Z. E. Abedin and S. Matter, *Phys. Chem. Chem. Phys.*, 2006, **8**, 2101-
390 2116.
391 49 X. K. He, B. L. Hou, C. Li, Q. Y. Zhu, Y. M. Jiang and L. Y. Wu, *Electrochim.*
392 *Acta*, 2014, **130**, 245-252.
393 50 P. Kedzierzawski and Z. Szklarska-Smialowska, *J. Electroanal. Chem.*, 1981, **122**,
394 269-278.
395 51 M. Frank and J. Winnick, *J. Electroanal. Chem.*, 1987, **238**, 163-182.
396 52 R. S. Nicholson, I. Shain, *Anal. Chem*., 1964, **36**, 706-723.
397 53 I. H. Plonski, *J. Electrochem. Soc.*, 1970, **117**, 1048-1052.
398 54 W. Le, K. Du, L. Zhang, J. Xiao, C. Zhang, Y. W. Zhang, L. Zhou and Q. Yin,
399 *Electrochim. Acta*, 2013, **95**, 179-184.
400 55 L. Wang, Y. L. Zheng, X. P. Lu, Z. Li, L. L. Sun and Y. H. Song, *Sensor. Actuat.*
401 *B-Chem.*, 2014, **195**, 1-7.

403 **Figure Captions**

404 **Fig. 1.** Cyclic voltammograms of pure [BMIM]$HSO_4$ (curve a) and 0.55 M Cr(III)-

405 [BMIM]$HSO_4$ (curve b) solutions on a GC electrode at 353 K. Scan rate is 50 $mV \cdot s^{-1}$.

406 **Fig. 2.** Cyclic voltammograms of 0.55 M Cr(III) on a GC electrode in [BMIM]$HSO_4$

407 solution at 353 K with different potential scanning rates between 50 and 250 $mV \cdot s^{-1}$

408 using the scan ranges from -0.2 to -2.45 V (a), -0.90 to -1.69 V (b) and -1.85 to -2.45

409 V (c).

410 **Fig. 3.** Peak potential $E_p$ vs. ln$v$ for Cr(III) reduction on a GC electrode in

411 [BMIM]$HSO_4$ solution at 353 K. (a-peak A, b-peak B)

412 **Fig. 4.** Peak current $I_{pA}$ vs. $v^{1/2}$ for Cr(III) reduction on a GC electrode in

413 [BMIM]$HSO_4$ solution at 353 K.

414 **Fig. 5.** Linear sweep voltammogram(a) and Tafel curve(b) for 0.55 M Cr(III) on a GC

415 electrode in [BMIM]$HSO_4$ solution at 353 K.

416 **Fig. 6.** SEM micrographs of chromium deposits on Cu substrate at 353 K for 30 min

417 from the 0.55 M Cr(III)-[BMIM]$HSO_4$ solution at -2.00 V: a × 5000, b × 10000. EDS

418 analysis (c) and XRD pattern (d) of the deposited layer.

419 **Fig. 7.** (a) Theoretical $\eta$-$t$ curves of two process reduction reaction,

420 (b) Chronopotentiograms of 0.55 M Cr(III) on a GC electrode in [BMIM]$HSO_4$

421 solution at 353 K.

422 **Fig. 8.** (a) Current-time transients of the chronoamperometry experiments recorded on

423 a GC electrode in 0.55 M Cr(III)-[BMIM]$HSO_4$ solution at 353 K. (b) Dimensionless

424 plots for instantaneous and progressive nucleation model in comparison with

425 experimental transients. (c) Plots of $I$ against $t^{-1/2}$ from the decreasing portion of

current-time transients in Fig. 8 (a) for the deposition process of 0.55 M Cr(III) on a GC electrode.

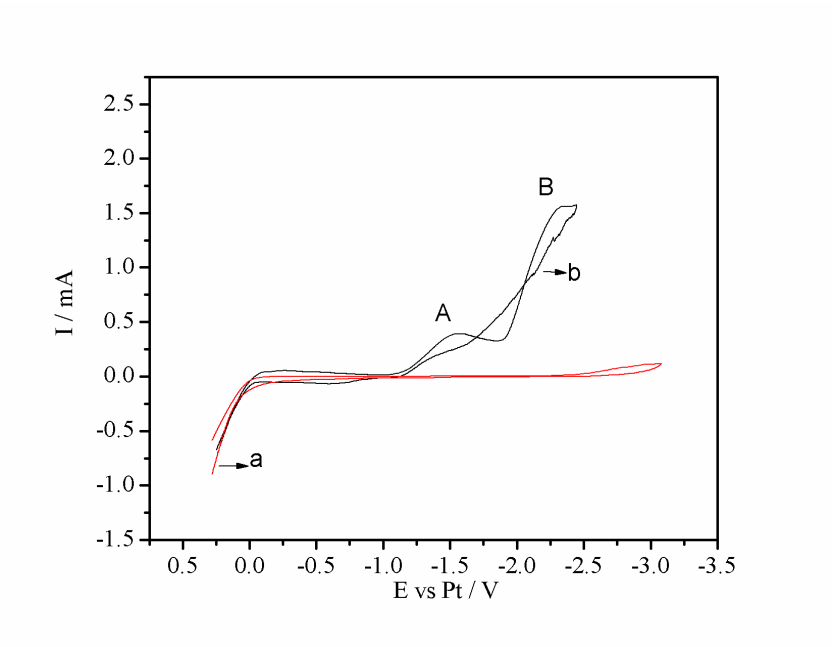


**Fig. 1** Cyclic voltammograms of pure [BMIM]$HSO_4$ (curve a) and 0.55 M Cr(III)-[BMIM]$HSO_4$ (curve b) solutions on a GC electrode at 353 K. Scan rate is 50 $mV \cdot s^{-1}$.

Xinkuai He, *et al.*, Fig. 1

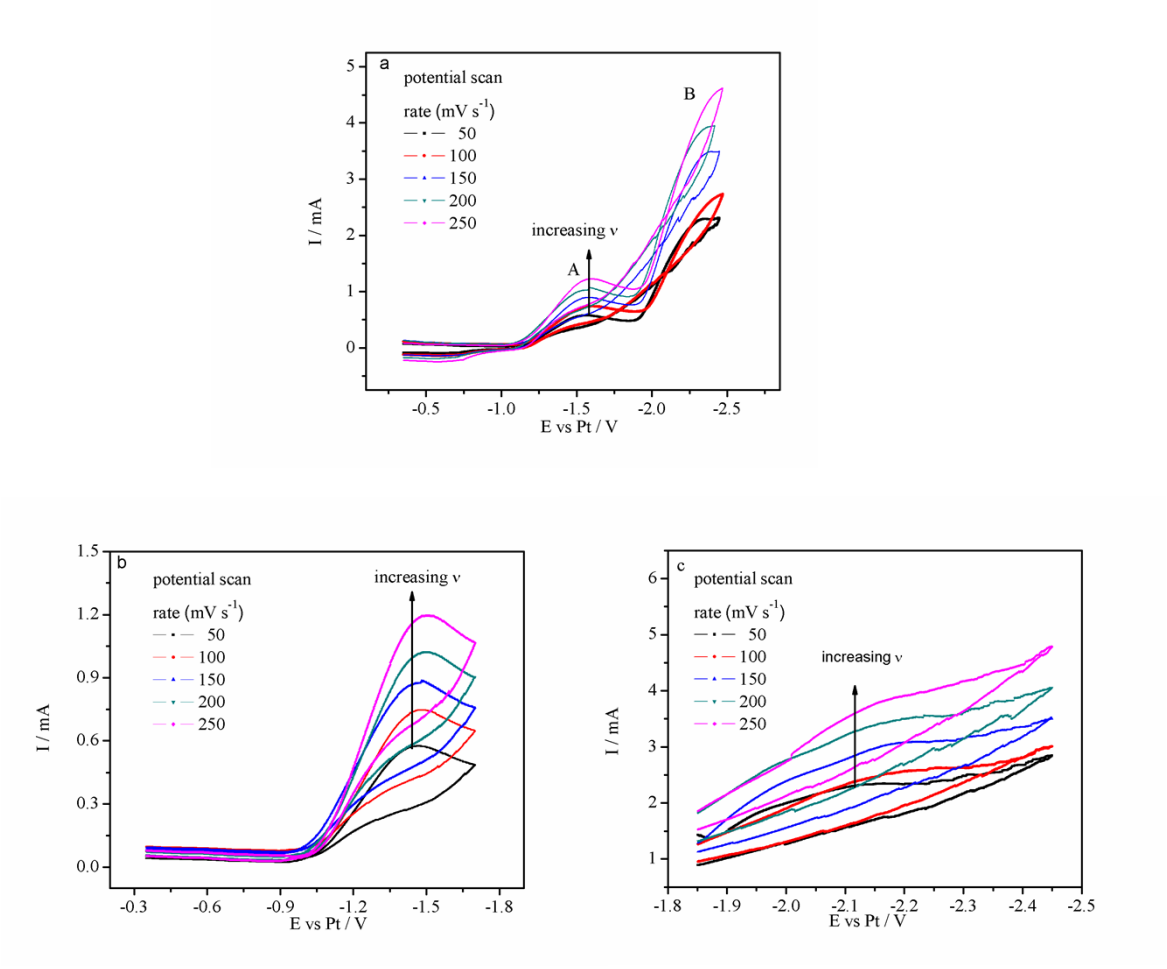


**Fig. 2** Cyclic voltammograms of 0.55 M Cr(III) on a GC electrode in [BMIM]$HSO_4$ solution at 353 K with different potential scanning rates between 50 and 250 mV·$s^{-1}$ using the scan ranges from -0.2 to -2.45 V (a), -0.90 to -1.69 V (b) and -1.85 to -2.45 V (c).

Xinkuai He, *et al.*, Fig. 2

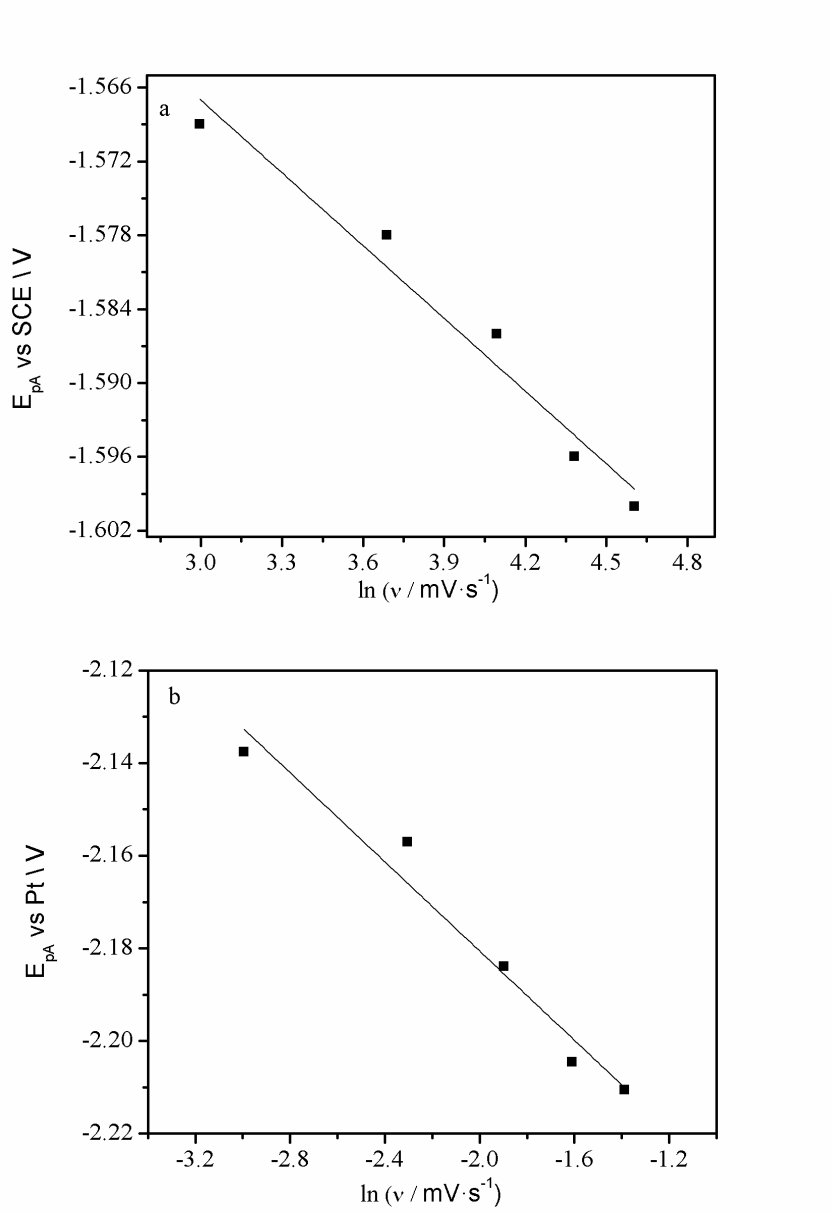


**Fig. 3** Peak potential $E_p$ vs. ln$v$ for Cr(III) reduction on a GC electrode in [BMIM]$HSO_4$ solution at 353 K. (a-peak A, b-peak B)

Xinkuai He, *et al.*, Fig. 3

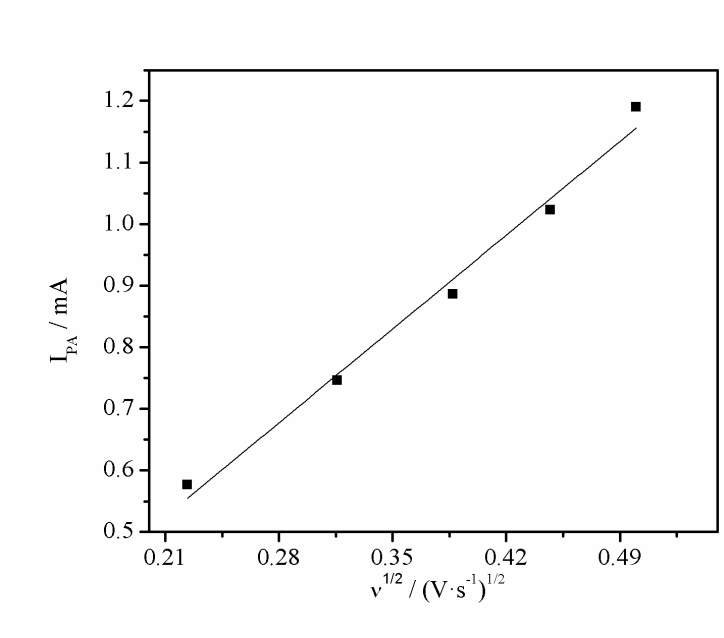


**Fig. 4** Peak current $I_{pA}$ vs. $v^{1/2}$ for Cr(III) reduction on a GC electrode in [BMIM]$HSO_4$ solution at 353 K.

Xinkuai He, *et al.*, Fig. 4

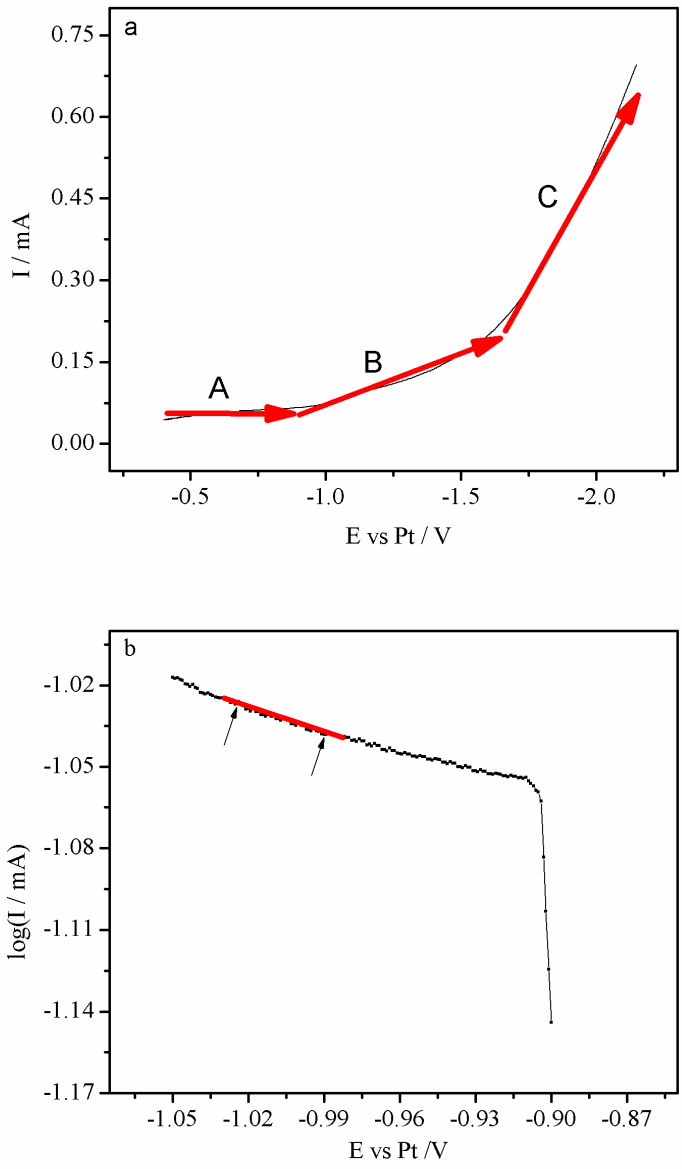


**Fig. 5** Linear sweep voltammogram(a) and Tafel curve(b) for 0.55 M Cr(III) on a GC electrode in [BMIM]$HSO_4$ solution at 353 K.

Xinkuai He, *et al.*, Fig. 5

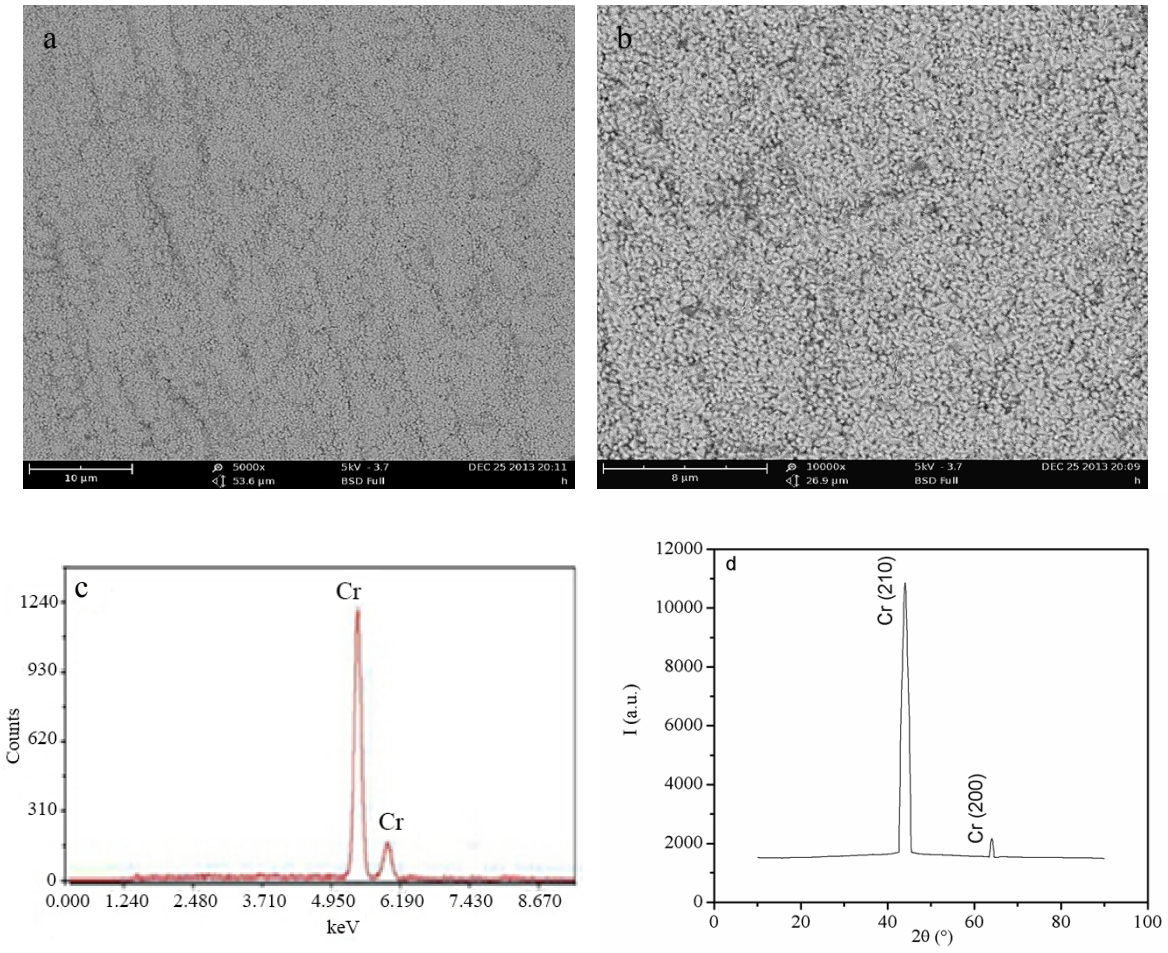


**Fig. 6** SEM micrographs of chromium deposits on Cu substrate at 353 K for 30 min from the 0.55 M Cr(III)-[BMIM]$HSO_4$ solution at -2.00 V: a × 5000, b × 10000. EDS analysis (c) and XRD pattern (d) of the deposited layer.

Xinkuai He, *et al.*, Fig. 6

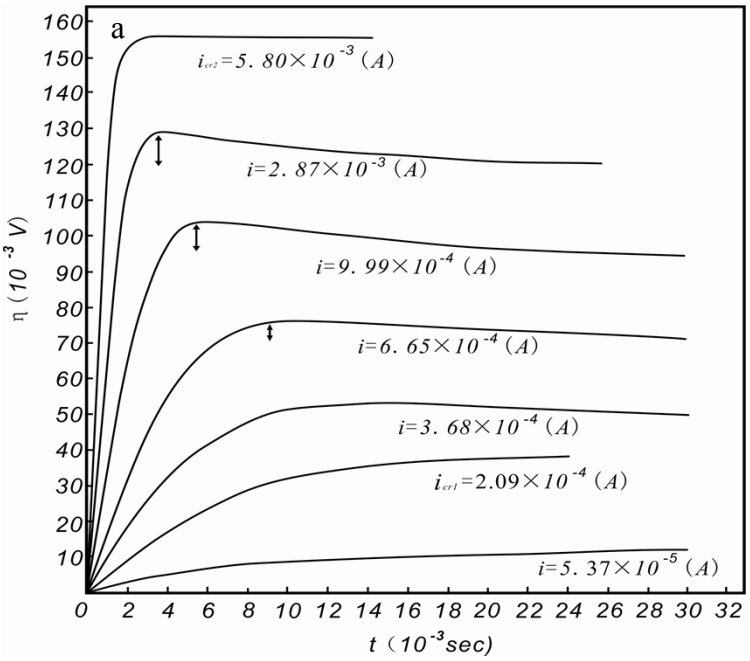


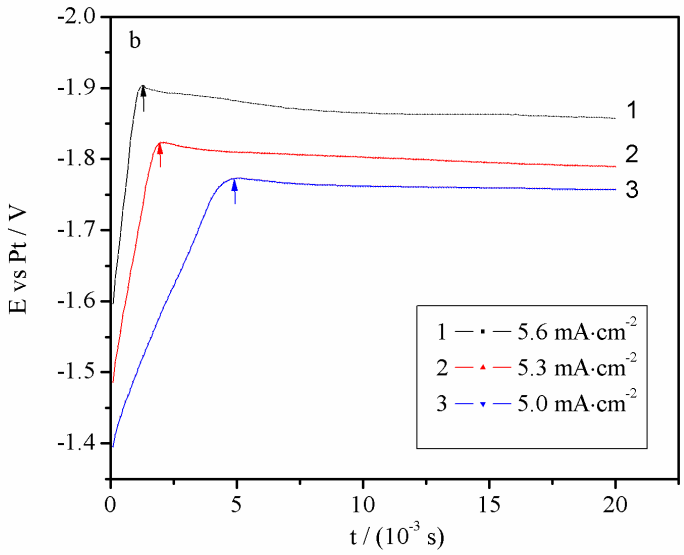


**Fig. 7** (a) Theoretical $\eta$-$t$ curves of two process reduction reaction, (b) Chronopotentiograms of 0.55 M Cr(III) on a GC electrode in [BMIM]$HSO_4$ solution at 353 K.

Xinkuai He, *et al.*, Fig. 7

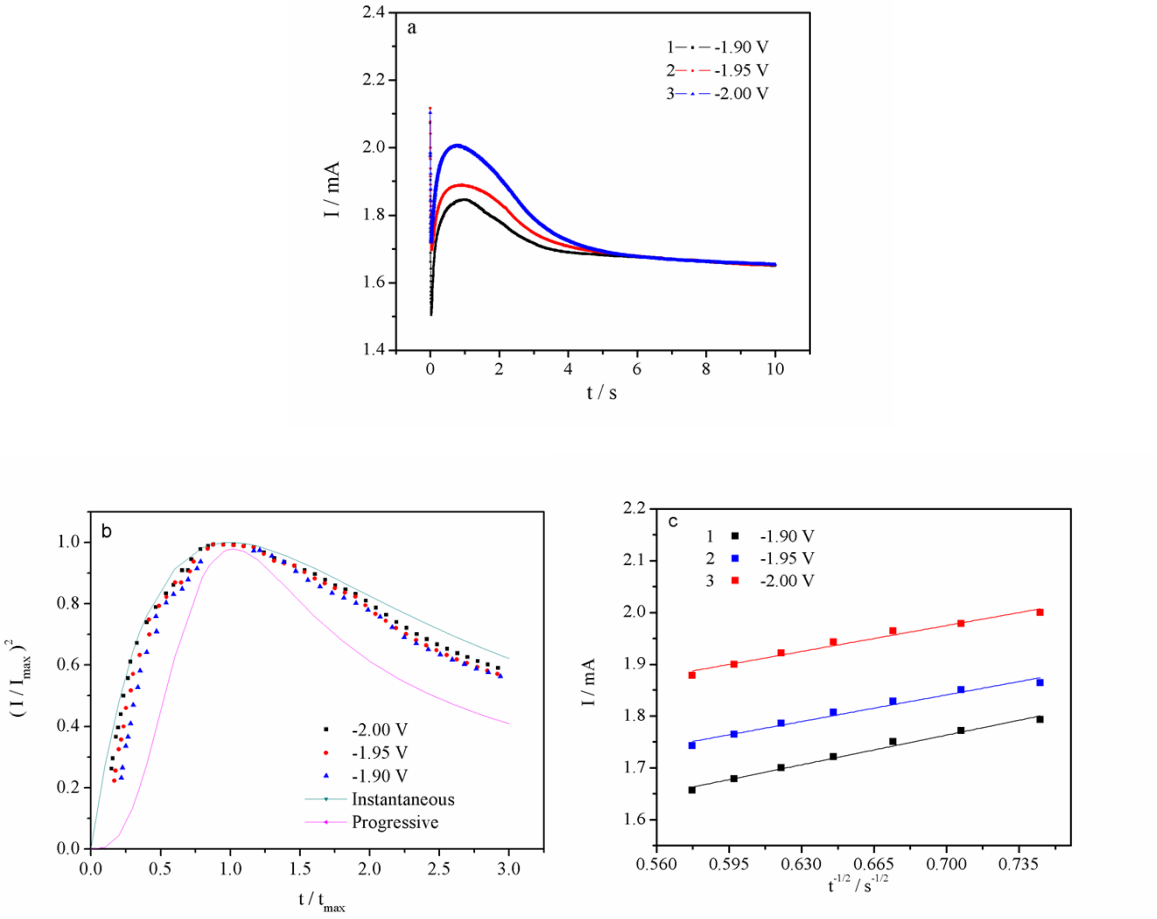


**Fig. 8** (a) Current-time transients of the chronoamperometry experiments recorded on a GC electrode in 0.55 M Cr(III)-[BMIM]$HSO_4$ solution at 353 K. (b) Dimensionless plots for instantaneous and progressive nucleation model in comparison with experimental transients. (c) Plots of $I$ against $t^{-1/2}$ from the decreasing portion of current-time transients in Fig. 8 (a) for the deposition process of 0.55 M Cr(III) on a GC electrode.

Xinkuai He, *et al.*, Fig. 8

# Electrochemical mechanism of Cr(III) reduction for preparing crystalline chromium coatings based on 1-butyl-3-methylimidazolium hydrogen sulfate ionic liquid

Xinkuai He, Chen Li, Qingyun Zhu, Bailong Hou, Yumei Jiang, Luye Wu *

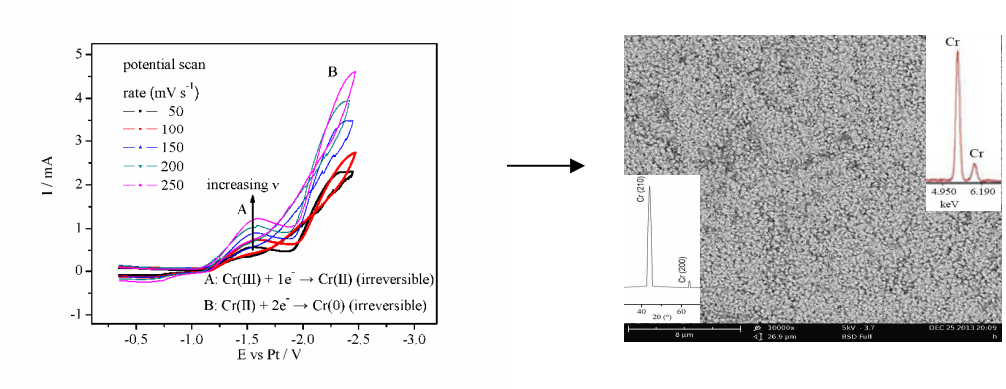


We report Cr(III) electrochemical reduction mechanism and nucleation/growth process, and the electrodepositing directly crystalline chromium coatings based on [BMIM]$HSO_4$.